First observation and study of the $K^\pm \to \pi^0\pi^0\mu^\pm\nu$ decay

The NA48/2 collaboration

E-mail: anna.korotkova@cern.ch, dmitry.madigozhin@cern.ch

ABSTRACT: The NA48/2 experiment at CERN reports the first observation of the $K^\pm \to \pi^0\pi^0\mu^\pm\nu$ decay based on a sample of 2437 candidates with 15% background contamination collected in 2003–2004. The decay branching ratio in the kinematic region of the squared dilepton mass above $0.03\,\mathrm{GeV}^2/c^4$ is measured to be $(0.65 \pm 0.03) \times 10^{-6}$. The extrapolation to the full kinematic space, using a specific model, is found to be $(3.45 \pm 0.16) \times 10^{-6}$, in agreement with chiral perturbation theory predictions.

https://doi.org/10.1007/JHEP03(2024)137

Contents

1 Introduction

Semileptonic four-body decays of kaons, $K^\pm \to \pi^{\pm,0}\pi^{\mp,0}l^\pm\nu$ (K_{l4}^{+-}, K_{l4}^{00}) with $l = e, \mu$, are of particular interest because of the small number of hadrons in the final state, which allows studying low energy QCD, while the electroweak amplitude responsible for the leptonic part is well-understood in the Standard Model. The development over more than 30 years of chiral perturbation theory (ChPT) [1, 2] has allowed predictions of form factors and decay rates at a precision level competitive with the accuracy of the experimental results in the electron modes [3–5]. In particular, the most recent theoretical works, prompted by the precise experimental measurements, have focused on form factor evaluation at higher orders, including radiative and isospin breaking effects, and developed a dispersive approach to match Low Energy Constants of ChPT [6, 7]. The muon modes are still to be investigated experimentally as the $\pi^+\pi^-$ mode observation relies on a few events [8] and the $\pi^0\pi^0$ mode has not been observed. This study reports the first observation and branching ratio (BR) measurement of the $K^\pm \to \pi^0\pi^0\mu^\pm\nu$ decay mode by the NA48/2 experiment at the CERN SPS.

2 Theoretical framework and available measurements

The differential rate of the K_{l4}^{00} decay may be parameterized in terms of the five Cabibbo-Maksymowicz variables [9] illustrated in figure 1: S_π, the squared mass of the dipion system; S_l, the squared mass of the dilepton system; θ_π, the angle of a pion direction in the dipion rest frame with respect to the dipion line of flight in the kaon rest frame; θ_l, the angle of the charged lepton direction in the dilepton rest frame with respect to the dilepton line
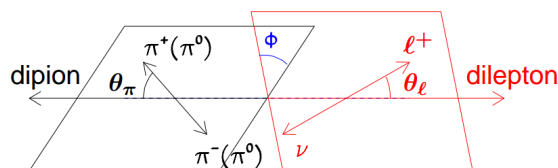
Figure 1. Cabibbo-Maksymowicz variables describing the semileptonic K_{l4}^{+-} (K_{l4}^{00}) decays.

of flight in the kaon rest frame; and ϕ, the angle between the dipion and dilepton planes in the kaon rest frame.

Unlike the K_{l4}^{+-} mode, where the definition of $\cos\theta_\pi$ and ϕ is driven by the π^+ meson, the final state with two neutral pions cannot favour one particular π^0. Integration over the $\cos\theta_\pi$ and ϕ variables leads to the simplified differential rate [2]

$$d\Gamma_3 = \frac{G_F^2|V_{us}|^2(1-z_l)^2\sigma_\pi X}{2^{11}\pi^5 m_{K^+}^5}(I_1 + I_2 \, \cos 2\theta_l + I_6 \, \cos\theta_l) \, dS_\pi dS_l d\cos\theta_l, \qquad (2.1)$$

where G_F is the Fermi coupling constant, V_{us} is the Cabibbo-Kobayashi-Maskawa matrix element, $z_l = m_l^2/S_l$, $\sigma_\pi = \sqrt{1 - 4m_{\pi^0}^2/S_\pi}$, $X = \frac{1}{2}\sqrt{\lambda(m_{K^+}^2, S_\pi, S_l)}$, and $\lambda(x,y,z) = x^2 + y^2 + z^2 - 2(xy + xz + yz)$ is the triangle function. The terms I_1, I_2, I_6 carry the dependence on the kinematic variables (S_π, S_l) and combinations of the complex hadronic form factors F_1, F_4. In contrast to the electron mode, terms including z_μ cannot be neglected and contribute to the decay amplitude:

$$I_1 = \{(1+z_\mu)|F_1|^2 + 2z_\mu|F_4|^2\}/4, \quad I_2 = -(1-z_\mu)|F_1|^2/4, \quad I_6 = z_\mu\Re(F_1^*F_4). \qquad (2.2)$$

The two complex hadronic form factors F_1, F_4 are functions of the real form factors F and R. Considering the isospin decomposition of F_1, F_4, the F, R form factors in the neutral pion (00) mode are related to those of the charged pion mode (+−) by: $(F,R)_{00} = -(F^+, R^+)_{+-}$, where (F^+, R^+) are the symmetric parts of (F,R). Using the notations P and L of the four-vector sum of the two pions and the four-vector sum of the two leptons, respectively, the form factors are written as $F_1 = -XF$ and $F_4 = (PL)F + S_\mu R$ in the neutral pion mode, under the assumption of no isospin violating contributions ($m_u = m_d = \alpha_{QED} = 0$).

The F form factor has been measured precisely by NA48/2 in the K_{e4}^{00} decay mode [5] and may be used in the $K_{\mu4}^{00}$ decay assuming lepton flavour universality. The dependence of F with $q^2 = S_\pi/4m_{\pi^+}^2 - 1$ and S_l ($l = e, \mu$) is

$$F(K_{l4}^{00}) = \begin{cases} 1 + aq^2 + bq^4 + c \cdot S_l/4m_{\pi^+}^2, & q^2 \geq 0 \\ 1 + d\sqrt{|q^2/(1+q^2)|} + c \cdot S_l/4m_{\pi^+}^2, & q^2 \leq 0 \end{cases} \qquad (2.3)$$

where $a = 0.149 \pm 0.033 \pm 0.014$, $b = -0.070 \pm 0.039 \pm 0.013$, $c = 0.113 \pm 0.022 \pm 0.007$, $d = -0.256 \pm 0.049 \pm 0.016$. In each case, the first error quoted is statistical and the second error is systematic. The F absolute normalization has been also measured as $F = f \cdot F(K_{e4}^{00})$, where $f = 6.079 \pm 0.012_{\text{stat}} \pm 0.027_{\text{syst}} \pm 0.046_{\text{ext}}$.

In contrast, the R form factor, which does not contribute to K_{e4} decays, has never been measured so far and only theoretical calculations exist at various orders of ChPT [2].
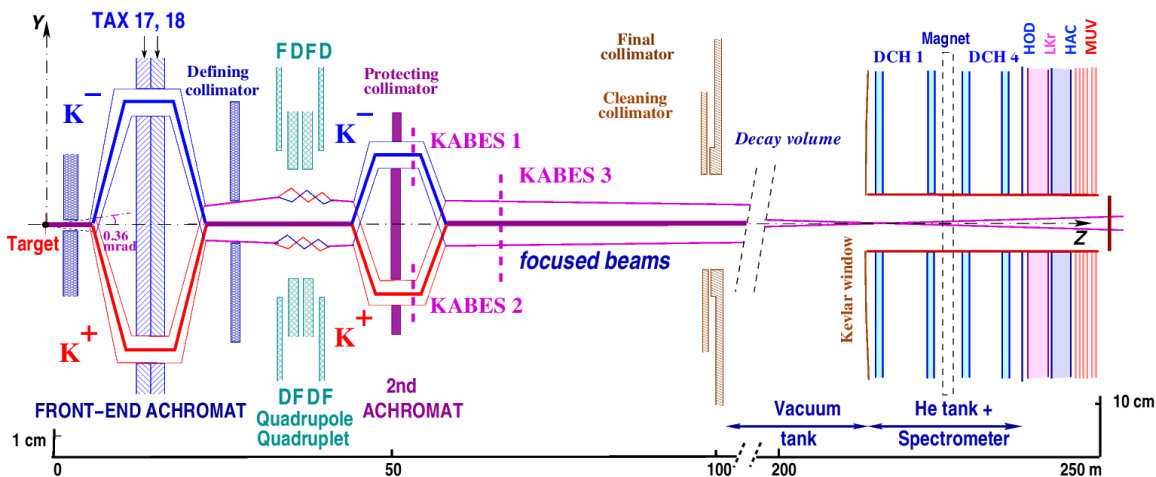
Figure 2. Schematic side view of the NA48/2 setup.

3 Beams and detectors

The NA48/2 experiment at the CERN SPS was designed to search for direct CP violation in $K^\pm$ decays to three pions [10]. During the 2003–2004 data taking period, the 400 GeV proton beam from the SPS was impinging on a beryllium target to produce simultaneous K^+ and K^- beams (figure 2). A front-end achromat separated locally positively and negatively charged beams in the vertical direction, allowing a dump-collimator (TAX 17, 18) with two holes, 20 cm apart, to select positive and negative particles with a central momentum of 60 GeV/c and a momentum band of 3.8% (rms). A second achromat separated again locally the positive and negative beams by 8 cm, allowing the three stations of the kaon beam spectrometer (KABES) [11] to measure the momentum of each individual particle. Each KABES station consisted of two time projection chambers using the MICROMEGAS technology [12]. The achieved resolutions were 800 μm, better than 1% and 600 ps for space point, momentum and time, respectively. At the exit of this achromat the beams traveled on a common axis towards the decay region. The two resulting beams, each 1 cm wide in the transverse plane, were superimposed in the decay volume enclosed in a 114 m long vacuum tank.

Charged products from the $K^\pm$ decays were measured by a magnetic spectrometer consisting of four drift chambers (DCH) and a dipole magnet located between the second and the third chamber. The spectrometer was located in a tank filled with helium at atmospheric pressure and separated from the decay volume by a thin Kevlar composite window. The magnet provided a transverse momentum kick of $\Delta p = 120$ MeV/c to charged particles in the horizontal plane. The spatial resolution of each DCH was $\sigma_x = \sigma_y = 90$ μm and the achieved momentum resolution was $\sigma_p/p = (1.02 \oplus 0.044 \cdot p)\%$ (p in GeV/c). The spectrometer was followed by a hodoscope (HOD) consisting of two planes of plastic scintillators segmented into horizontal and vertical strips and arranged in four quadrants.

A liquid krypton calorimeter (LKr) located behind the HOD was used to reconstruct $\pi^0 \rightarrow \gamma\gamma$ decays. It was an almost homogeneous ionization chamber with an active volume of about 10 m^3 of liquid krypton, segmented transversely into 13248 projective cells, 2×2 cm^2 each. The calorimeter energy resolution was $\sigma_E/E = (3.2/\sqrt{E} \oplus 9/E \oplus 0.42)\%$ (E in GeV).

The LKr was followed by a hadronic calorimeter (HAC) with a total iron thickness of 1.2 m. A Muon Veto system (MUV), consisting of three layers made of 80 cm iron followed by scintillators, was used to identify muons. A detailed description of the NA48 detector and its performance has been published in [13].

The experiment collected a total of 1.2×10^{10} triggers in two years of data-taking using a dedicated two-level trigger logic to select and flag events. In the study reported here, a sub-sample of 2×10^8 triggers is considered: the first level trigger required a signal in at least one HOD quadrant in coincidence with the presence of energy deposits in LKr consistent with at least two photons. At the second level, an on-line processor receiving the DCH information reconstructed the momentum of charged particles and calculated the missing mass to the $(K^\pm - \pi^\pm)$ system under the assumption that the particles were $\pi^\pm$ originating from the decay of a $60\,\mathrm{GeV}/c$ $K^\pm$ traveling along the nominal beam axis. The requirement that the missing mass exceeds the π^0 mass was imposed to reject most $K^\pm \to \pi^\pm \pi^0$ decays (the lower trigger cutoff was $194\,\mathrm{MeV}/c^2$ in 2003 and $181\,\mathrm{MeV}/c^2$ in 2004).

4 Event reconstruction and selection

The signal branching ratio $\mathrm{BR}(K_{\mu4}^{00})$ is measured relative to the abundant normalization channel $K^\pm \to \pi^0 \pi^0 \pi^\pm$ $(K_{3\pi}^{00})$, which leads to identical numbers of detected charged and neutral particles and is collected concurrently through the same trigger logic:

$$\mathrm{BR}(K_{\mu4}^{00}) = \frac{N_S}{N_N} \cdot \frac{A_N}{A_S} \cdot K_\mathrm{trig} \cdot \mathrm{BR}(K_{3\pi}^{00}), \tag{4.1}$$

where N_N and N_S are the numbers of selected events after background subtraction in the normalization and signal samples, respectively; the corresponding selection acceptances A_N and A_S are computed using a detailed GEANT3-based [14] Monte Carlo simulation (MC); and K_trig is a factor accounting for possible differences in the trigger efficiency between the signal and normalisation samples. The kinematic cut applied at the second trigger level is fully efficient for both $K_{\mu4}^{00}$ and $K_{3\pi}^{00}$ decays. The normalization branching ratio is $\mathrm{BR}(K_{3\pi}^{00}) = (1.760 \pm 0.023)\%$ [15].

A common selection is considered, followed by exclusive criteria to distinguish normalization and signal candidates. The common selection includes a charged and a neutral selection.

The charged selection requires a DCH track with momentum P_DCH in the range 5–$35\,\mathrm{GeV}/c$ and the distance between the track and the beam axis in the DCH1 plane larger than 12 cm; at least one KABES track with momentum P_KABES in the range 54–$67\,\mathrm{GeV}/c$, within 10 ns of the DCH track time and carrying the same charge as the DCH track. The best matching KABES track and the DCH track are propagated to the closest point of approach to define the charged vertex with longitudinal position Z_c.

The neutral selection requires four photon candidates defined as energy deposits in the LKr calorimeter larger than $3\,\mathrm{GeV}/c$, separated by at least 2 cm from any inactive cell, by at least 10 cm from any other photon candidate in-time within 5 ns, and by at least 15 cm from the extrapolated position at the LKr front plane of any DCH track with an associated HOD time within 10 ns of any photon candidate. Each of the photon candidates should be within 2.5 ns of the four-photon average time. The four candidates should be consistent with the decay

of two neutral pions at longitudinal positions Z_1 and Z_2, obtained under the assumption that each pair of photons is produced by a $\pi^0 \to \gamma\gamma$ decay, with $|Z_1 - Z_2| < 500$ cm. The neutral vertex position is defined as the average of the two π^0 vertex positions: $Z_n = (Z_1 + Z_2)/2$, and is required to be in a 106 m long decay region upstream of DCH1.

Combinations with $|Z_n - Z_c| < 600$ cm are considered further. In case several combinations satisfy this condition, the one with the smallest discriminant value is selected. The discriminant D_{nc} takes into account the resolution of $Z_1 - Z_2$ and $Z_n - Z_c$ according to

$$D_{nc} = \left(\frac{Z_1 - Z_2}{\sigma_{12}(Z_n)}\right)^2 + \left(\frac{Z_n - Z_c}{\sigma_{nc}(Z_{av})}\right)^2, \tag{4.2}$$

where σ_{12}, σ_{nc} are the Gaussian widths of the $Z_1 - Z_2$ and $Z_n - Z_c$ distributions, measured on data and parameterized as a function of Z_n and $Z_{av} = (Z_n + Z_c)/2$, respectively.

Each candidate is reconstructed in the $(m_{3\pi}, P_t)$ plane, where $m_{3\pi}$ is the mass of the three pion system (assuming a π^+ mass for the DCH track) and P_t is its transverse momentum relative to the nominal beam axis. The $K^{00}_{3\pi}$ normalization candidates are required to be inside an ellipse centred at the kaon mass and P_t value of $5\,\mathrm{MeV}/c$, with semi-axes $10\,\mathrm{MeV}/c^2$ and $20\,\mathrm{MeV}/c$, respectively, thus ensuring fully reconstructed $K^{00}_{3\pi}$ three-body decays (figure 3).

The selection of $K^{00}_{\mu4}$ signal candidates requires the reconstructed $m_{3\pi}$ and P_t values to be outside the $K^{00}_{3\pi}$ ellipse. Additional conditions are applied to identify a muon in the final state and suppress the contribution of $K^{00}_{3\pi}$ with a decay in flight $\pi^\pm \to \mu^\pm \nu$ which mimics the signal kinematics. Muon identification requires the deflected DCH track, extrapolated to the MUV plane, to be within the instrumented area and spatially associated to a MUV signal. A condition $P_{DCH} > 10\,\mathrm{GeV}/c$ is applied to ensure high muon identification efficiency.

The missing mass squared variable m^2_{miss} used to discriminate signal and background candidates is evaluated using the 4-momenta of all measured particles:

$$m^2_{miss} = (E_K - E_{\pi^0_1} - E_{\pi^0_2} - E_\mu)^2 - (\vec{P}_{KABES} - \vec{P}_{\pi^0_1} - \vec{P}_{\pi^0_2} - \vec{P}_{DCH})^2, \tag{4.3}$$

where $E_K = \sqrt{P^2_{KABES} + m^2_{K^+}}$ and $E_\mu = \sqrt{P^2_{DCH} + m^2_\mu}$ are the kaon and muon energies, respectively. In a similar way, $m^2_{miss}(\pi)$ is defined as a squared missing mass reconstructed assigning the charged pion mass m_{π^+} to the DCH track instead of m_μ.

Values of $m^2_{miss}(\pi)$ close to zero correspond to a $K^{00}_{3\pi}$ decay kinematics. Due to the correlation between the reconstructed $m^2_{miss}(\pi)$ and m^2_{miss} values, a selection condition is applied in the $(m^2_{miss}(\pi), m^2_{miss})$ plane, $m^2_{miss}(\pi) < 0.5 m^2_{miss} - 0.0008\ \mathrm{GeV}^2/c^4$, to reject the $K^{00}_{3\pi}$ decays in the signal sample (figure 4).
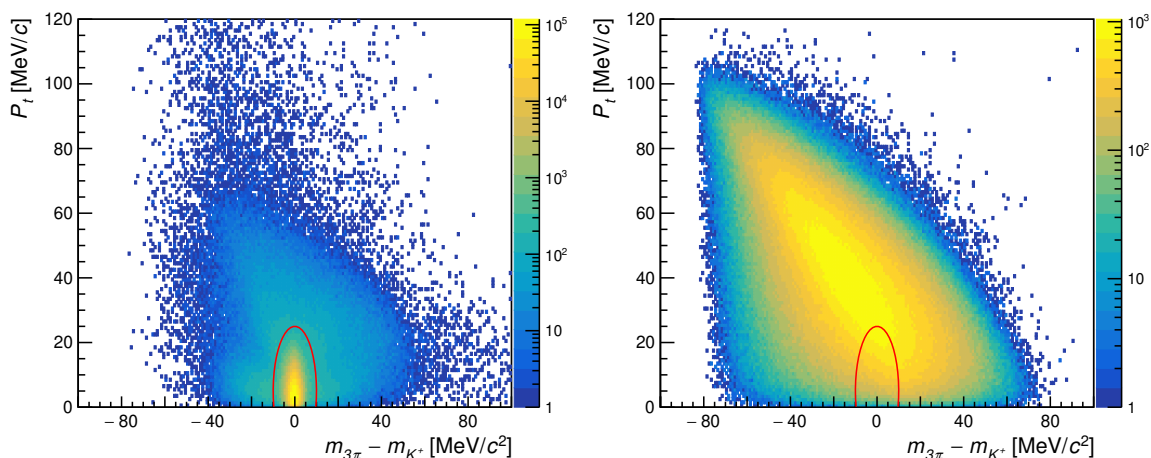
Figure 3. Distribution of simulated events in the reconstructed $(m_{3\pi} - m_{K^+}, P_t)$ plane after the common selection, for $K_{3\pi}^{00}$ decays (left) and $K_{\mu 4}^{00}$ decays (right). Events within the ellipse are selected as normalization candidates. Events outside the ellipse are selected as signal candidates.
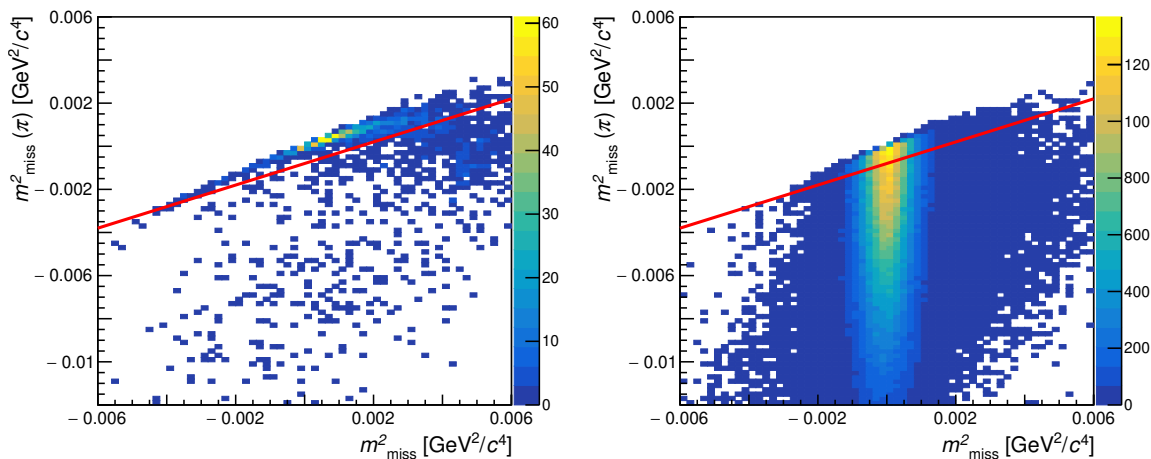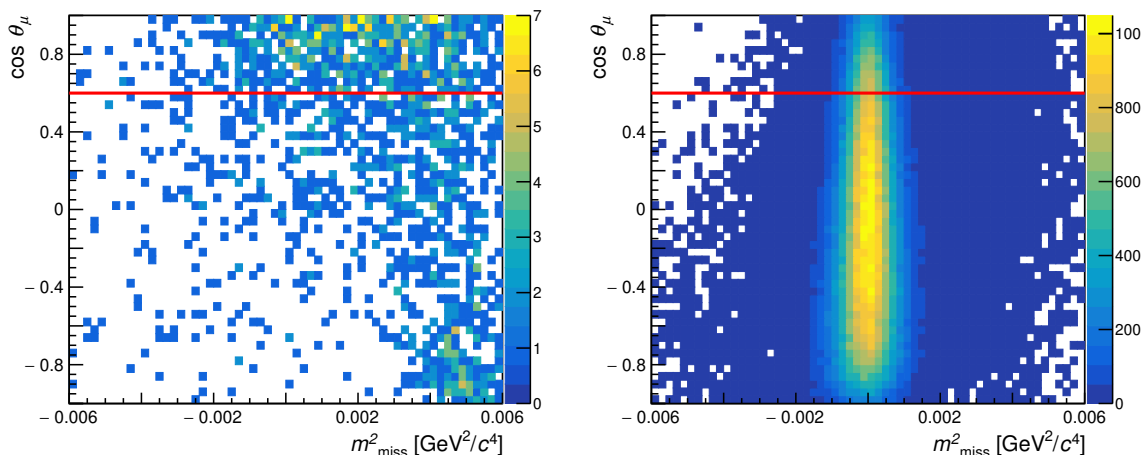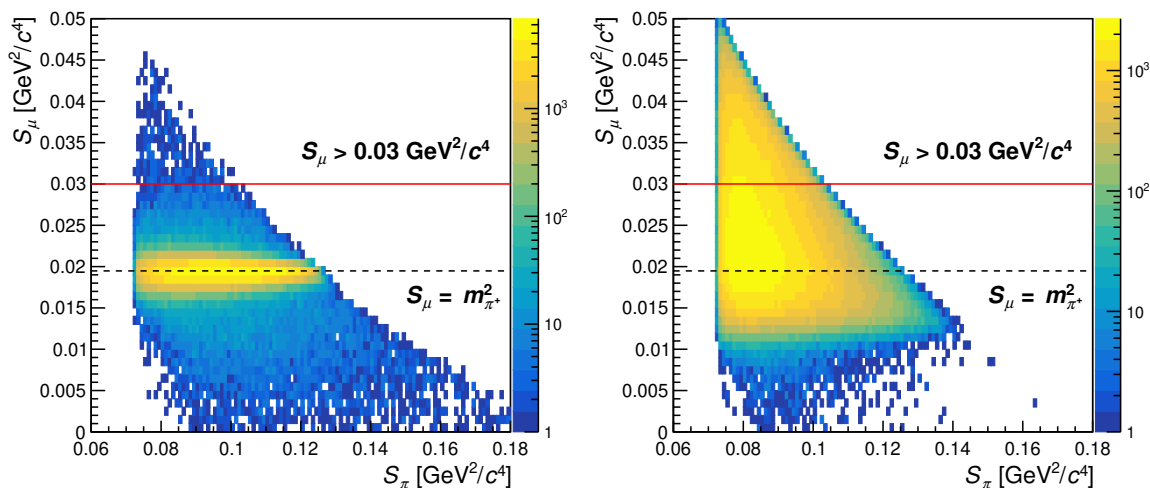

Figure 4. Distributions of simulated $K_{3\pi}^{00}$ background (left) and $K_{\mu 4}^{00}$ signal candidates (right) in the reconstructed $(m_{\mathrm{miss}}^2, m_{\mathrm{miss}}^2(\pi))$ plane after the signal selection, but before applying the condition in this plane. Candidates above the line are excluded.
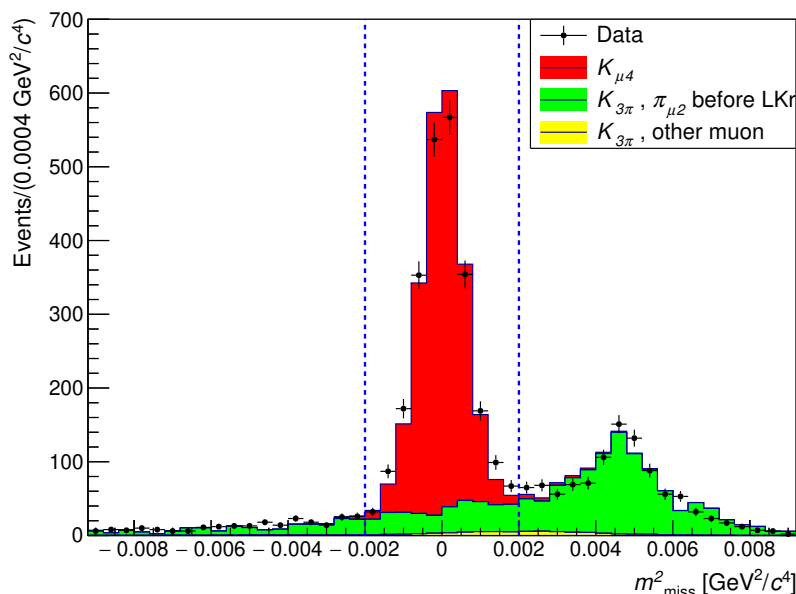
Figure 5. Distribution of simulated $K_{3\pi}^{00}$ background (left) and $K_{\mu4}^{00}$ signal candidates (right) in the reconstructed $(m_{\text{miss}}^2, \cos\theta_\mu)$ plane after the signal selection, but before applying the condition in this plane. Candidates above the line are excluded.

Figure 6. Distributions of simulated $K_{3\pi}^{00}$ background (left) and $K_{\mu4}^{00}$ signal candidates (right) in the reconstructed (S_π, S_μ) plane after the signal selection, but before applying the condition in this plane. Candidates above the solid line are selected.

Figure 7. Distribution of m^2_{miss} for the selected data events (markers), simulated background and signal contributions (histograms). Vertical lines show the signal region.

Residual background from the $K^{00}_{3\pi}$ decay followed by $\pi^\pm \to \mu^\pm \nu$ decay is suppressed by requiring $\cos\theta_\mu < 0.6$ (figure 1 with $l = \mu$), as expected from the different shapes of the signal and $K^{00}_{3\pi}$ background distributions (figure 5). The background is suppressed further by requiring that the reconstructed dilepton mass, computed as the squared missing mass to the dipion system, satisfies the condition $S_\mu > 0.03\,\text{GeV}^2/c^4$ (figure 6). The $K^{00}_{3\pi}$ events reconstructed with $S_\mu > 0.03\,\text{GeV}^2/c^4$ are due to possible mis-reconstruction of the track when the pion decays in the spectrometer, or an association to a mis-reconstructed π^0 pair, as shown by simulations.

Applying the signal selection to the data sample leads to 3718 $K^{00}_{\mu4}$ signal candidates, of which 2437 lie in the signal region $|m^2_{\text{miss}}| < 0.002\,\text{GeV}^2/c^4$. The regions $|m^2_{\text{miss}}| > 0.002\,\text{GeV}^2/c^4$ are used as control regions in the background evaluation. The normalization channel conditions select 7.3×10^7 $K^{00}_{3\pi}$ reconstructed data events. The normalization sample is considered as background-free. A possible relative contamination from K^{00}_{e4} and $K^{00}_{\mu4}$ decays is below 10^{-4} and gives a negligible contribution to the uncertainty on the signal BR measurement.

5 Background evaluation

The background from $K^{00}_{3\pi}$ decays followed by pion decays upstream of the LKr front plane is evaluated by simulation. The background from $K^{00}_{3\pi}$ decays with the pion decaying or interacting in the LKr calorimeter and leading to a muon signal is evaluated from control data samples. A method was developed to predict the m^2_{miss} shape of these contributions, using the pion track measured in the DCH spectrometer.

A control data sample is obtained by applying the $K^{00}_{\mu4}$ signal selection, excluding the requirement of an associated MUV signal and requiring a pion-like energy deposit E_{LKr} in the LKr calorimeter such that $0.3 < E_{\mathrm{LKr}}/P_{\mathrm{DCH}} < 0.8$. This sample corresponds to secondary pions produced in hadronic interactions and decaying to low-energy muons. Another sample is obtained by weighting each event by the momentum-dependent decay probability, which corresponds to energetic pions decaying downstream of the LKr front plane before interacting.

The m^2_{miss} spectra of data events, and those of simulated signal and estimated backgrounds, are shown in figure 7. The $K^{00}_{\mu4}$ signal is observed as a peak in the m^2_{miss} distribution. The background contributions are obtained from a fit of the two distributions to the data in the control m^2_{miss} region, excluding the signal region and taking into account the simulated signal tails. The contribution from $K^{00}_{3\pi}$ decays with the pion decaying or interacting in the LKr calorimeter, labeled "other muon" in figure 7, is found to be ten times smaller than the main background component. The number of background events in the signal region is found to be $354 \pm 33_{\mathrm{stat}}$ by integrating the background contributions.

6 Acceptances

The MC simulation is used to compute the selection acceptance for signal and normalization channels. The simulation includes full detector geometry and material description, detector local inefficiencies and misalignment, accurate simulation of the kaon beam line and time variations of the above throughout the data taking period. The muon identification efficiency is emulated according to the measurement using a $K^{00}_{3\pi}$ data sample selected by inverting the neutral and charged vertex matching condition and requiring S_μ to be consistent with $m^2_{\pi^+}$, thus ensuring a $\pi^\pm \to \mu^\pm \nu$ decay. The measured efficiency is parameterized as a function of the track momentum and distance from the beam axis in the MUV plane. Applying this model to simulated signal events, the integrated MUV inefficiency is found to be 1.65%.

The signal channel $K^{00}_{\mu4}$ is simulated according to [2] including the *1-loop* description of the form factor R and the form factor F measured in the K^{00}_{e4} mode (eq. 2.3). The signal region definition $|m^2_{\mathrm{miss}}| < 0.002\,\mathrm{GeV}^2/c^4$ contains 98.2% of the selected MC events (figure 7). The resulting acceptance is $A_S = (3.453 \pm 0.007_{\mathrm{stat}})\%$ in the restricted kinematic space $S_\mu > 0.03\,\mathrm{GeV}^2/c^4$ and is $A_S = (0.651 \pm 0.001_{\mathrm{stat}})\%$ in the full kinematic space.

The normalization channel $K^{00}_{3\pi}$ is generated using the measured decay amplitude [16] implemented using an empirical parameterization of the data [17]. The normalization acceptance is evaluated as $A_N = (4.477 \pm 0.002_{\mathrm{stat}})\%$. The statistical uncertainties quoted are related to the sizes of the simulated samples and have a negligible impact on the measurement.

7 Systematic uncertainties and results

The last ingredient needed by eq. (4.1) is the trigger correction K_{trig}. Because of the similar topology of the signal and normalization decay modes, most inefficiencies, measured using control triggers from data or MC emulations, cancel at first order and lead to $K_{\mathrm{trig}} = 0.999 \pm 0.002$. The uncertainty in the measured K_{trig} factor is propagated as a systematic contribution.

The systematic uncertainty related to the background evaluation is estimated by considering alternative methods: neglecting the smaller of the two background components; restricting the control region to $m_{\text{miss}}^2 > 0.004\,\text{GeV}^2/c^4$; and adding extra smearing to the signal distribution. The largest deviation from the reference value is quoted as a systematic uncertainty, leading to $354 \pm 33_{\text{stat}} \pm 62_{\text{syst}}$ background events in the signal region.

The systematic uncertainties related to accidental in-time signals are estimated by enlarging by a factor of two the time windows used for coincidence of KABES and DCH tracks, consistency of HOD track time and LKr photon times, and of the four LKr photon candidates. The contribution is conservatively calculated as a linear sum of the unsigned shifts induced by the extension of each considered time window.

The systematic uncertainty related to the MUV inefficiency modelling in the simulation is quoted as 20% of its effect on the signal acceptance calculation, which reflects its maximum variation when applying tighter and looser selection conditions of the $K_{3\pi}^{00}$ data sample used in the evaluation.

The signal acceptance depends on the form factor description used in the simulation (section 2). The related uncertainty is estimated by weighting the simulated events according to the corresponding variations of the differential rate. Several modifications are investigated including replacing the description of R_{1-loop} by R_{tree} [2]; modifying the relative contribution of F and R by 20% at the reference point $(S_\pi = 4m_{\pi^+}^2, S_\mu = m_\mu^2)$; varying each parameter of $F(K_{e4}^{00})$ within its uncertainty. Conservatively, all observed variation are added in quadrature.

Stability checks, considering data sub-samples defined by the kaon beam charge and data taking period do not reveal any evidence for residual systematic effects.

Table 1 summarizes the achieved measurement in the kinematic space $S_\mu > 0.03\,\text{GeV}^2/c^4$, $\text{BR}(K_{\mu4}^{00}) = (0.65 \pm 0.02_{\text{stat}} \pm 0.02_{\text{syst}} \pm 0.01_{\text{ext}}) \times 10^{-6}$, together with the detailed uncertainties. The branching ratio measurement precision is dominated by the statistics of the signal sample and the uncertainty in the background evaluation. As expected, the branching ratio in the full kinematic space, $\text{BR}(K_{\mu4}^{00}) = (3.45 \pm 0.10_{\text{stat}} \pm 0.11_{\text{syst}} \pm 0.05_{\text{ext}}) \times 10^{-6}$, is more sensitive to the form factor modelling than the branching ratio in the restricted space: the corresponding uncertainty is 1.37% , leading to a total systematic uncertainty of 3.30% and a total error of 4.55%. All other components are scaled according to their relative contributions $\delta\text{BR}/\text{BR}$.

The S_π and S_μ distributions of the selected events are shown in figure 8 together with simulated signal and backgrounds. The limited kinematic space accessible does not allow a measurement of the R form factor, while the observed agreement between data and simulation confirms a reasonable quality of the model used for the signal acceptance calculation.

As the signal acceptance depends on the form factor model considered, the same data are used to extract the branching ratio under different assumptions. The comparison of the NA48/2 measurement with the corresponding theoretical predictions is shown in figure 9. The three lower predicted values of $\text{BR}(K_{\mu4}^{00})$ correspond to the *tree* level, *1-loop* and "beyond *1-loop*" models of the form factors F and R, respectively [2]. The "beyond *1-loop*" model uses R_{1-loop} and includes the F form factor measurement [18] obtained by the S118 experiment at the CERN PS using a sample of 30 000 K_{e4}^{+-} decays. The other three values correspond to our evaluation of the predicted branching ratio using the $F(K_{e4}^{00})$ measurement of NA48/2 [5] and three models of R: $R = R_{1-loop}$ from [2], $R = 0$ and $R = 2 \times R_{1-loop}$, respectively.

BR($K^{00}_{\mu4}$) central value [10^{-6}]	0.651	
	δBR[10^{-6}]	δBR/BR
Data statistical error	0.019	2.85%
MC statistical error	0.001	0.21%
Trigger	0.001	0.18%
Background	0.019	2.96%
Accidentals	0.002	0.32%
MUV inefficiency	0.002	0.33%
Form factor modelling	0.001	0.14%
Total systematic error	0.020	3.01%
BR($K^{00}_{3\pi}$) error (external)	0.009	1.31%
Total error	0.028	4.35%

Table 1. Result of the BR($K^{00}_{\mu4}$) measurement in the restricted kinematic space $S_\mu > 0.03\,\mathrm{GeV}^2/c^4$ and contributions of the considered uncertainties.
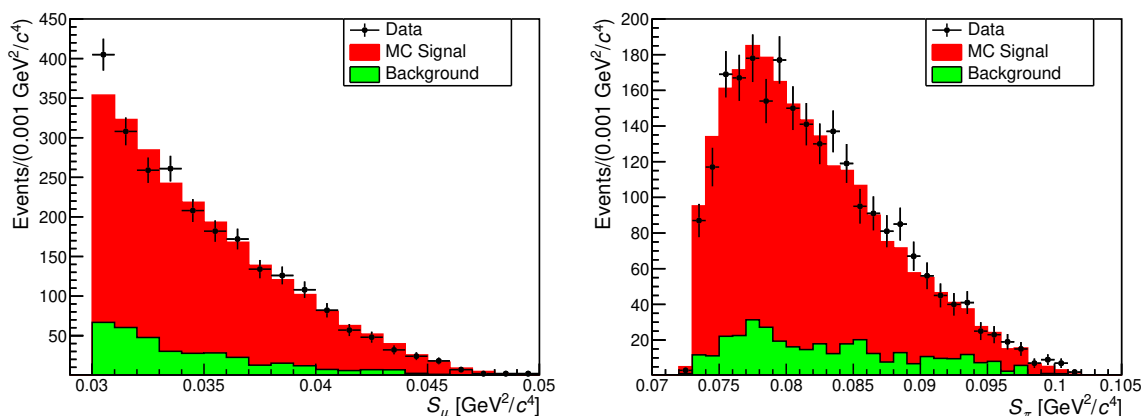
Figure 8. Distributions of S_μ and S_π variables for data (markers), signal simulation and background estimation (histograms) for $S_\mu > 0.03\,\mathrm{GeV}^2/c^4$.

The agreement of the measured branching ratio and the predicted value improves when introducing more elaborate models of the form factors. The data do not support the simple models of F and R form factors (*tree* and *1-loop* models) and are in agreement with the most recent F measurement and R_{1-loop} calculation. The achieved NA48/2 measurement is not precise enough to determine the variation of R with S_π and S_μ.

8 Conclusion

The NA48/2 experiment at CERN reports the first observation of the $K^{\pm} \to \pi^0\pi^0\mu^{\pm}\nu$ decay from a sample of 2437 signal candidates with 15% background contamination. Measure-

ments of the branching ratio are obtained in the kinematic region $S_\mu > 0.03\,\mathrm{GeV}^2/c^4$ as $\mathrm{BR}(K_{\mu4}^{00}) = (0.65 \pm 0.02_{\mathrm{stat}} \pm 0.02_{\mathrm{syst}} \pm 0.01_{\mathrm{ext}}) \times 10^{-6} = (0.65 \pm 0.03) \times 10^{-6}$, and extrapolated to the full kinematic space as $\mathrm{BR}(K_{\mu4}^{00}) = (3.45 \pm 0.10_{\mathrm{stat}} \pm 0.11_{\mathrm{syst}} \pm 0.05_{\mathrm{ext}}) \times 10^{-6} = (3.45 \pm 0.16) \times 10^{-6}$, using a form factor model based on experimental measurements and ChPT calculations. The results are consistent with a contribution of the R form factor, as computed at *1-loop* ChPT. The restricted kinematic region considered in this study, $S_\mu > 0.03\,\mathrm{GeV}^2/c^4$, does not allow a more precise measurement of the R form factor description.
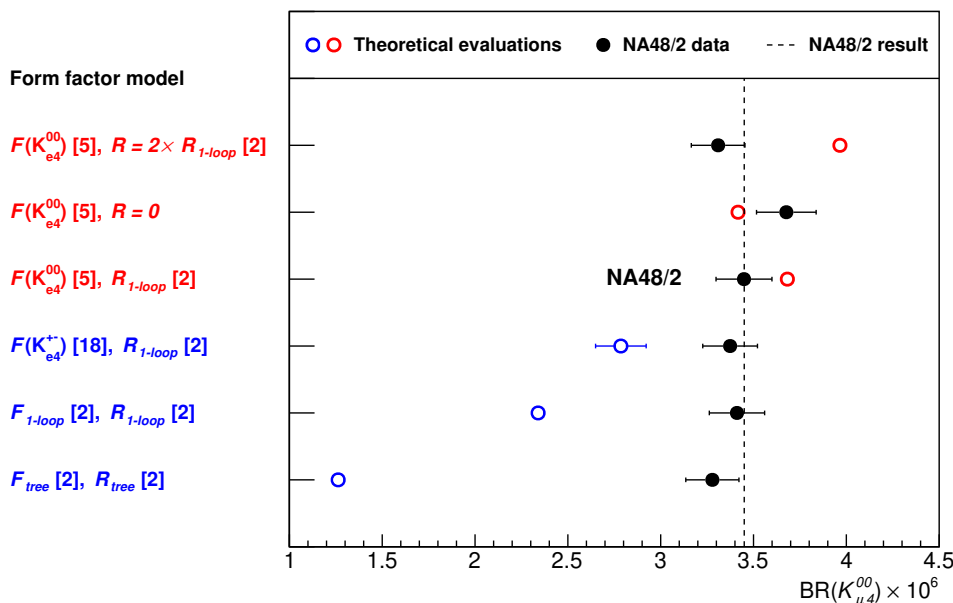
Figure 9. Evolution of the theoretical evaluation of the branching fraction $\mathrm{BR}(K_{\mu4}^{00})$ with the form factor model considered (open markers) and comparison with the NA48/2 measurement using the corresponding model in the selection acceptance calculation (solid markers). The theoretical evaluations obtained using F and R form factors from ChPT in [2] are labeled as blue open markers. The theoretical evaluations obtained by replacing the F description from [18] by the more precise measurement of [5] are labeled as red open markers. The NA48/2 measurement is most consistent with the theoretical evaluation considering the ChPT formulation R_{1-loop}.

Acknowledgments

References

[1] S. Weinberg, *Phenomenological Lagrangians*, *Physica A* **96** (1979) 327 [INSPIRE].

[2] J. Bijnens, G. Colangelo and J. Gasser, K_{l4} *decays beyond one loop*, *Nucl. Phys. B* **427** (1994) 427 [`hep-ph/9403390`] [INSPIRE].

[3] NA48/2 collaboration, *Precise tests of low energy QCD from K_{e4} decay properties*, *Eur. Phys. J. C* **70** (2010) 635 [INSPIRE].

[4] NA48/2 collaboration, *New measurement of the charged kaon semileptonic $K^{\pm} \to \pi^+ \pi^- e^{\pm} \nu$ (K_{e4}) decay branching ratio and hadronic form factors*, *Phys. Lett. B* **715** (2012) 105 [*Addendum ibid.* **740** (2015) 364] [`arXiv:1206.7065`] [INSPIRE].

[5] NA48/2 collaboration, *Detailed study of the $K^{\pm} \to \pi^0 \pi^0 e^{\pm} \nu$ (K_{e4}^{00}) decay properties*, *JHEP* **08** (2014) 159 [`arXiv:1406.4749`] [INSPIRE].

[6] V. Bernard, S. Descotes-Genon and M. Knecht, *On some aspects of isospin breaking in the decay $K^{\pm} \to \pi^0 \pi^0 e^{\pm} \overset{(-)}{\nu_e}$*, *Eur. Phys. J. C* **75** (2015) 145 [`arXiv:1501.07102`] [INSPIRE].

[7] G. Colangelo, E. Passemar and P. Stoffer, *A dispersive treatment of $K_{\ell 4}$ decays*, *Eur. Phys. J. C* **75** (2015) 172 [`arXiv:1501.05627`] [INSPIRE].

[8] V. Bisi, R. Cester, A. Marzari-Chiesa and M. Vigone, K^+ *rare decay modes*, *Phys. Lett. B* **25** (1967) 572 [INSPIRE].

[9] N. Cabibbo and A. Maksymowicz, *Angular correlations in K_{e4} decays and determination of low-energy π-π phase shifts*, *Phys. Rev.* **137** (1965) B438 [*Erratum ibid.* **168** (1968) 1926] [INSPIRE].

[10] NA48/2 collaboration, *Search for direct CP violating charge asymmetries in $K^{\pm} \to \pi^{\pm} \pi^+ \pi^-$ and $K^{\pm} \to \pi^{\pm} \pi^0 \pi^0$ decays*, *Eur. Phys. J. C* **52** (2007) 875 [`arXiv:0707.0697`] [INSPIRE].

[11] B. Peyaud, *KABES: a novel beam spectrometer for NA*48, *Nucl. Instrum. Meth. A* **535** (2004) 247 [INSPIRE].

[12] Y. Giomataris, P. Rebourgeard, J.P. Robert and G. Charpak, *MICROMEGAS: a high granularity position sensitive gaseous detector for high particle flux environments*, *Nucl. Instrum. Meth. A* **376** (1996) 29 [INSPIRE].

[13] NA48 collaboration, *The beam and detector for the NA*48 *neutral kaon CP violations experiment at CERN*, *Nucl. Instrum. Meth. A* **574** (2007) 433 [INSPIRE].

[14] R. Brun et al., *GEANT detector description and simulation tool*, CERN-W5013, CERN, Geneva, Switzerland (1994) [`DOI:10.17181/CERN.MUHF.DMJ1`] [ɪɴSPIRE].

[15] Pᴀʀᴛɪᴄʟᴇ Dᴀᴛᴀ Gʀᴏᴜᴘ collaboration, *Review of particle physics*, *PTEP* **2022** (2022) 083C01 [ɪɴSPIRE].

[16] NA48/2 collaboration, *Determination of the S-wave $\pi\pi$ scattering lengths from a study of $K^{\pm} \to \pi^{\pm}\pi^0\pi^0$ decays*, *Eur. Phys. J. C* **64** (2009) 589 [`arXiv:0912.2165`] [ɪɴSPIRE].

[17] NA48/2 collaboration, *Empirical parameterization of the $K^{\pm} \to \pi^{\pm}\pi^0\pi^0$ decay Dalitz plot*, *Phys. Lett. B* **686** (2010) 101 [`arXiv:1004.1005`] [ɪɴSPIRE].

[18] L. Rosselet et al., *Experimental study of* 30,000 K_{e4} *decays*, *Phys. Rev. D* **15** (1977) 574 [ɪɴSPIRE].

The NA48/2 collaboration

Cavendish Laboratory, University of Cambridge, Cambridge, United Kingdom

J.R. Batley [iD], G. Kalmus, C. Lazzeroni [iD][1], D.J. Munday[1], M.W. Slater [iD][1], S.A. Wotton [iD]

CERN, Genève, Switzerland

R. Arcidiacono [iD][2], G. Bocquet, N. Cabibbo[†], A. Ceccucci [iD], D. Cundy[3], V. Falaleev [iD][4],
M. Fidecaro [iD][†], L. Gatignon [iD][5], A. Gonidec, W. Kubischta, A. Maier, A. Norton [iD][6], M. Patel[7],
A. Peters

The Enrico Fermi Institute, The University of Chicago, Chicago, U.S.A.

E. Monnier [iD][8], E. Swallow[†], R. Winston[9]

Department of Physics and Astronomy, University of Edinburgh, Edimburgh, United Kingdom

P. Rubin [iD][10], A. Walker

Dipartimento di Fisica e Scienze della Terra dell'Università e Sezione dell'INFN di Ferrara, Ferrara, Italy

P. Dalpiaz, C. Damiani, M. Fiorini [iD], M. Martini, F. Petrucci [iD], M. Savrié [iD], M. Scarpa,
H. Wahl [iD][11]

Sezione dell'INFN di Ferrara, Ferrara, Italy

W. Baldini [iD], A. Cotta Ramusino [iD], A. Gianoli [iD]

Dipartimento di Fisica, Università di Firenze e Sezione dell'INFN di Firenze, Sesto Fiorentino, Italy

M. Calvetti, E. Celeghini, E. Iacopini [iD], M. Lenti [iD], G. Ruggiero [iD]

Sezione dell'INFN di Firenze, Sesto Fiorentino, Italy

A. Bizzeti [iD][12], M. Veltri [iD][13]

Institut für Physik, Universität Mainz, Mainz, Germany

M. Behler, K. Eppard, M. Hita-Hochgesand, K. Kleinknecht, P. Marouelli, L. Masetti [iD],
U. Moosbrugger, C. Morales Morales, B. Renk, M. Wache, R. Wanke [iD], A. Winhart

Department of Physics and Astronomy, Northwestern University, Evanston, U.S.A.

0000-0002-1619-3121

D. Coward [iD][14], A. Dabrowski [iD][15], T. Fonseca Martin, M. Shieh, M. Szleper [iD][16], M. Velasco,
M.D. Wood[14]

Dipartimento di Fisica dell'Università e Sezione dell'INFN di Perugia, Perugia, Italy

G. Anzivino [iD], E. Imbergamo, A. Nappi[†], M. Piccini [iD], M. Raggi [iD][17], M. Valdata-Nappi

Sezione dell'INFN di Perugia, Perugia, Italy

P. Cenci ⓘ, M. Pepe ⓘ, M.C. Petrucci

Dipartimento di Fisica dell'Università e Sezione dell'INFN di Pisa, Pisa, Italy

F. Costantini ⓘ, N. Doble ⓘ[11], L. Fiorini ⓘ[18], S. Giudici ⓘ, G. Pierazzini[†], M. Sozzi ⓘ, S. Venditti

Scuola Normale Superiore e Sezione dell'INFN di Pisa, Pisa, Italy

G. Collazuol ⓘ[19], L. Di Lella ⓘ[11], G. Lamanna ⓘ[20], I. Mannelli ⓘ, A. Michetti

Sezione dell'INFN di Pisa, Pisa, Italy

C. Cerri, R. Fantechi ⓘ

DSM/IRFU — CEA Saclay, Gif-sur-Yvette, France

B. Bloch-Devaux ⓘ[21], C. Cheshkov[22], J.B. Chèze, M. De Beer, J. Derré, G. Marel, E. Mazzucato, B. Peyaud, B. Vallage

Fachbereich Physik, Universität Siegen, Siegen, Germany

M. Holder, M. Ziolkowski ⓘ

Dipartimento di Fisica dell'Università e Sezione dell'INFN di Torino, Torino, Italy

S. Bifani ⓘ, M. Clemencic ⓘ[15], S. Goy Lopez ⓘ[23]

Sezione dell'INFN di Torino, Torino, Italy

C. Biino ⓘ, N. Cartiglia ⓘ, F. Marchetto ⓘ

Österreichische Akademie der Wissenschaften, Institut für Hochenergiephysik, Wien, Austria

H. Dibon, M. Jeitler ⓘ, M. Markytan, I. Mikulec ⓘ, G. Neuhofer, L. Widhalm[†]

Authors affiliated with an international laboratory covered by a cooperation agreement with CERN

S. Balev[†], P.L. Frabetti, E. Gersabeck ⓘ[24], E. Goudzovski ⓘ[1], P. Hristov ⓘ[15], V. Kekelidze ⓘ, A. Korotkova[*], V. Kozhuharov ⓘ[25], L. Litov ⓘ[25], D. Madigozhin ⓘ[*], N. Molokanova, I. Polenkevich, Yu. Potrebenikov ⓘ, S. Stoynev ⓘ[26], A. Zinchenko[†]

[*] *Corresponding author.*

[†] *Deceased*

[1] *Present address: School of Physics and Astronomy, University of Birmingham, Birmingham, B15 2TT, U.K.*

[2] *Also at Università degli Studi del Piemonte Orientale, I-13100 Vercelli, Italy*

[3] *Present address: Istituto di Cosmogeofisica del CNR di Torino, I-10125 Torino, Italy*

[4] *Present address: Sezione dell'INFN di Perugia, I-06100 Perugia, Italy*

[5] *Present address: Physics Department, University of Lancaster, Lancaster, LA1 4YW, U.K.*

[6] *Present address: School of Physics and Astronomy, University of Glasgow, Glasgow, G12 8QQ, U.K.*

[7] *Present address: Physics Department, Imperial College London, London, SW7 2BW, U.K.*

[8] *Present address: Centre de Physique des Particules de Marseille, Université Aix Marseille, CNRS/IN2P3, F-13288, Marseille, France*

[9] *Present address: University of California, Merced, CA 95344, U.S.A.*

[10] *Present address: George Mason University, Fairfax, VA 22030, U.S.A.*

[11] *Present address: Institut für Physik, Universität Mainz, D-55099 Mainz, Germany*

[12] *Also at Dipartimento di Scienze Fisiche, Informatiche e Matematiche, Università di Modena e Reggio Emilia, I-41125 Modena, Italy*

[13] *Also at Istituto di Fisica, Università di Urbino, I-61029 Urbino, Italy*

[14] *Present address: SLAC National Accelerator Laboratory, Stanford University, Menlo Park, CA 94025, U.S.A.*

[15] *Present address: CERN, CH-1211 Genève 23, Switzerland*

[16] *Present address: National Center for Nuclear Research, Swierk, P-05-400, Poland*

[17] *Present address: Università di Roma La Sapienza, Roma, Italy*

[18] *Present address: Instituto de Física Corpuscular IFIC, Universitat de València, E-46071 València, Spain*

[19] *Present address: Dipartimento di Fisica dell'Università e Sezione dell'INFN di Padova, I-35131 Padova, Italy*

[20] *Present address: Dipartimento di Fisica dell'Università e Sezione dell'INFN di Pisa, I-56100 Pisa, Italy*

[21] *Present address: Dipartimento di Fisica dell'Università, I-10125 Torino, Italy*

[22] *Present address: Institut de Physique Nucléaire de Lyon, IN2P3-CNRS, Université Lyon I, F-69622 Villeurbanne, France*

[23] *Present address: Centro de Investigaciones Energeticas Medioambientales y Tecnologicas, E-28040 Madrid, Spain*

[24] *Present address: School of Physics and Astronomy, The University of Manchester, Manchester, M13 9PL, U.K.*

[25] *Present address: Faculty of Physics, University of Sofia, 1164 Sofia, Bulgaria*

[26] *Present address: Fermi National Accelerator Laboratory, Batavia, IL 60510, U.S.A.*